HAL
open science

Ice crystal shapes in cirrus clouds derived from POLDER/ADEOS-1

Hélène Chepfer, Philippe Goloub, Jérôme Riédi, J. F. de Haan, J. W. Hovenier, P.-H. Flamant

To cite this version:

Hélène Chepfer, Philippe Goloub, Jérôme Riédi, J. F. de Haan, J. W. Hovenier, et al.. Ice crystal shapes in cirrus clouds derived from POLDER/ADEOS-1. Journal of Geophysical Research, 2001, 106 (D8), pp.7955-7966. 10.1029/2000JD900285 . hal-00811814

HAL Id: hal-00811814

https://hal.science/hal-00811814v1

Submitted on 11 Jan 2021

HAL is a multi-disciplinary open access archive for the deposit and dissemination of scientific research documents, whether they are published or not. The documents may come from teaching and research institutions in France or abroad, or from public or private research centers.

L'archive ouverte pluridisciplinaire **HAL**, est destinée au dépôt et à la diffusion de documents scientifiques de niveau recherche, publiés ou non, émanant des établissements d'enseignement et de recherche français ou étrangers, des laboratoires publics ou privés.

JOURNAL OF GEOPHYSICAL RESEARCH, VOL. 106, NO. D8, PAGES 7955-7966, APRIL 27, 2001

Ice crystal shapes in cirrus clouds derived from POLDER/ADEOS-1

H. Chepfer,[1] P. Goloub,[2] J. Riedi,[2] J.F. De Haan,[3] J.W. Hovenier,[3,4] and P. H. Flamant[1]

Abstract. This paper discusses the retrieval of ice crystal shapes of cirrus clouds on a global scale using observations collected with POLDER-1 (POLarization and Directionality of the Earth Reflectance) onboard the ADEOS-1 platform. The retrieval is based on polarized bidirectional observations made by POLDER. First, normalized polarized radiances are simulated for cirrus clouds composed of ice crystals that differ in shape and are randomly oriented in space. Different values of cloud optical depths, viewing geometries and solar zenith angles are used in the simulations. This sensitivity study shows that the normalized polarized radiance is highly sensitive to the shape of the scatterers for specific viewing geometries, and that it saturates after a few scattering events, which makes it rapidly independent of the optical depth of the cirrus clouds. Next, normalized polarized radiance observations obtained by POLDER have been selected, based on suitable viewing geometries and on the occurrence of thick cirrus clouds composed of particles randomly oriented in space. For various ice crystal shapes these observations are compared with calculated values pertaining to the same geometry, in order to determine the shape that best reproduces the measurements. The method is tested fully for the POLDER data collected on January 12, 1997. Thereafter, it is applied to six periods of 6 days of observations obtained in January, February, March, April, May, and June 1997. This study shows that the particle shape is highly variable with location and season, and that polycrystals and hexagonal columns are dominant at low latitudes, whereas hexagonal plates occur more frequently at high latitudes.

1. Introduction

Cirrus clouds cover permanently more than 20% of the Earth [*Warren* 1986, 1988 ; *Liao et al.*, 1995], and their impact on the Earth-atmosphere-ocean radiation balance is still an open question. They affect the radiative budget through two opposite effects: (1) they partly reflect the solar radiation thereby cooling the atmosphere, and (2) they partly block the terrestrial radiation, and this greenhouse effect tends to heat the atmosphere. Currently, neither of these two effects is correctly quantified for all regions of the Earth. Hence the impact of cirrus clouds on the global radiative budget is still poorly known [*Liou*, 1986 ; *Stephens et al.*, 1990]. Several parameters need to be studied to improve the radiative transfer properties of cirrus clouds in numerical models used for climate studies. These parameters are, for example, global cirrus cloud cover, cloud height, temperature, geometrical structure, optical depth, ice water content, and microphysical properties (i.e., ice crystal size, shape, and orientation in space).

During the last two decades, several intensive field experiments have been organized to study cirrus cloud properties on a local scale: FIRE I (First ISCCP Regional Experiment FIRE) and II (see the special issues of *Monthly Weather Review*, 1990, and *Journal of Atmospheric Science*, 1995), [*Arnott et al.*, 1991] took place in the United States in 1986 and 1991, ICE (International Cloud Experiment) [*Francis et al.*, 1994 ; *Brogniez et al.*, 1995] and EUCREX (European Cloud Radiation Experiment) [*Raschke* 1996, *Raschke et al.*, 1998] were performed in Europe in 1991, 1993, and 1994, CEPEX (Central Equatorial Pacific Experiment) [*McFarquar and Heymsfield* 1996] was executed in the Pacific Ocean in 1993, and SUCCESS (SUbsonic Aircraft Contrail and Cloud Effects Special Study) [special section *Geophysical Research Letter* 1998] took place in the United States in 1996. These experiments increased our understanding of cirrus cloud processes on a mesoscale and they pointed out a strong connection between the microphysical properties and the radiative impact of cirrus clouds.

On the basis of the results obtained during those intensive field programs, and work conducted in parallel, several groups have started to consider the retrieval of cirrus cloud properties from space observations. As cirrus cloud properties vary spatially (latitude and longitude) and temporally (lifetime and seasons), a complete description of the cirrus properties on a global scale requires satellite observations.

Minnis [1998] has summarized the needs and the state of the art of the retrieval of cirrus cloud parameters from satellite observations. Several authors [*Inoue* 1985 ; *Parol et al.*, 1991; *Minnis et al.*, 1993 ; *Giraud et al.*, 1997] have derived ice crystal size using the split window technique applied to IR channels and apriori ice crystal shape. More recently, *Baran et al.* [1999] deduced the particle size and shape using a dual view instrument, namely ATSR observations at 3.7 μm and 10.8 μm. Moreover, *Rolland and Liou* [1998] have studied the possibilities of deriving microphysical parameters of cirrus clouds using the MODIS instrument that was recently launched on EOS-AM.

[1] Laboratoire de Météorologie Dynamique, Palaiseau, France.

[2] Laboratoire d'Optique Atmosphérique, Villeneuve d'Ascq, France.

[3] Department of Physics and Astronomy, Free University of Amsterdam, The Netherlands.

[4] Also at Astronomical Institute "Anton Pannekoek" , University of Amsterdam, The Netherlands.

Copyright 2001 by the American Geophysical Union.

Paper number 2000JD900285
0148-0227/01/2000JD900285$09.00

In the present paper we present results of retrieving ice crystal shapes on a global scale using POLDER-1/ADEOS-1 data. This work is a first attempt to retrieve the particle shape from polarized bidirectional observations in the visible domain. The POLDER instrument characteristics are presented in section 2. In section 3 the ice crystal shapes considered in this study are discussed, as well as the radiative transfer code used to compute the normalized polarized radiance. Section 4 is devoted to the definition of criteria that will be used to select POLDER data suitable for the retrieval of ice crystal shape. In section 5, results of 1 day of observations are first presented as a test case, and then results of analyzing six periods of 6 days of POLDER observations are presented. Section 6 summarizes the results and discusses the limitations of the method used. The conclusions as well as possible future improvements are given in section 7.

2. POLDER Instrument

The POLDER instrument [*Deschamps et al.*, 1994] has been designed to measure normalized total radiances (L_n) and normalized polarized radiances ($L_{n,p}$) at the top of the atmosphere. The POLDER-1 instrument on ADEOS-1 performed measurements for 8 months, from November 1, 1996 to June 30, 1997, and the POLDER-2 instrument is scheduled for launch on ADEOS-2 in 2001. POLDER contains a CCD matrix of 242 x 274 pixels. The pixel resolution in the nadir direction is equal to 6.2 km x 6.2 km. Each fixed target is seen several times in different viewing geometries by the POLDER matrix, and the maximum number of different directions in which one target can be seen during an ADEOS overpass is 14.

The viewing directions observed with POLDER correspond to scattering angles between 60° and 180°, depending on the solar zenith angle and the position of ADEOS with respect to the position of the target. POLDER measures normalized radiances in eight different wavelength channels, some of which have been dedicated to the study of various atmospheric constituents, such as aerosols [*Herman et al.*, 1997; *Deuzé et al.*, 1998], clouds [*Buriez et al.*, 1997], and water vapor [*Vesperini et al.*, 2000], while others are used for studying ground properties like vegetation [*Leroy et al.*, 1997] and ocean color. The state of polarization of the light reflected by the atmosphere is measured in three different channels (443 nm, 670 nm, and 865 nm). The accuracy of the normalized polarized radiance is 0.001.

The importance of polarization measurements for remote sensing application has been pointed out by *Van de Hulst* [1957] and *Hansen* [1971] and, more recently, with regard to the POLDER instrument, by *Herman et al.* [1997]. The POLDER instrument provides not only, as do other instruments [*Diner at al.*, 1999], multiangle observations but also polarized radiance data. On the other hand, the spatial resolution (6.2x6.2 km^2) is comparatively coarse. Figures 1a and 1b show a POLDER image of a cirrus cloud over the ocean in total radiance and polarized radiance, respectively. Studies of cirrus cloud properties using POLDER data started with observations collected with an airborne simulator during intensive field experiments. The first results concerned the discrimination between ice and liquid water clouds by *Goloub et al.* [1994] and the determination of ice crystal shape and orientation in space [*Chepfer et al.*, 1998]. More recently, these studies have been extended to a global scale with POLDER-1/ADEOS-1 observations [*Goloub et al.*, 2000 and *Chepfer et al.*, 1999].

a

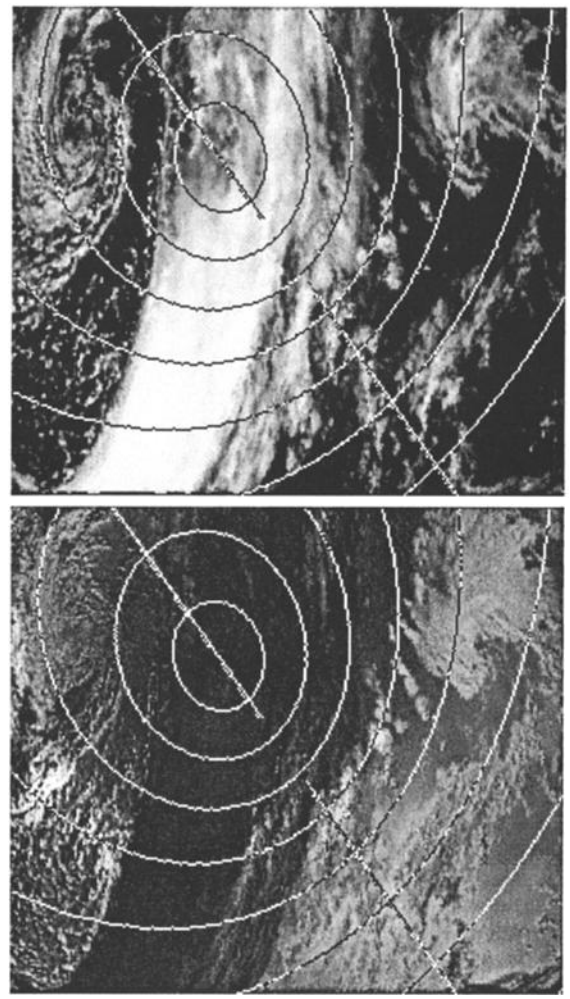

b

Figure 1. POLDER image (1700x1500 km^2) of a cirrus cloud over the North Pacific Ocean (May 9, 1997) in (a) radiance and (b) polarized radiance. The wavelength is 864 nm. The line corresponds to the solar principal plane and the curves denote the scattering angle with a 10° increment between each line. (c) Viewing geometry of the POLDER instrument.

3. Simulations of Bidirectional Polarized Reflectances

3.1. Models

In contrast to low-level liquid clouds, ice clouds can be composed of particles with shapes much more complex than spheres. In situ observations, collected during intensive field experiments such as FIRE, ICE, EUCREX, CEPEX, SUCCESS, have shown a high variability and sometimes a high complexity of ice crystal shapes [e.g. *Heymsfield*, 1975 ; *Krupp*, 1991 ; *Miloshevich and Heymsfield*, 1996). They also showed that the shape of the crystals depends on latitude, altitude, and on the conditions during formation of the cirrus clouds. These ice crystal shapes are sometimes simple, like plates or columns with a hexagonal base, and sometimes very complicated, like bullet rosettes or dendritic particles. The hexagonal structure is regularly observed, which is consistent with the fact that liquid

water naturally solidifies in a hexagonal structure. On the basis of these local observations we have selected various typical ice crystal shapes to study the sensitivity of polarized radiance with respect to the particle shape. The selected shapes are (1) simple ice crystals, like columns and plates, with a shape ratio $Q_{sr}=L/2R$ (L is the length of the crystal, and R is the radius of the circumscribed hexagonal base) which ranges from 0.05 to 2.5 [*Wendling et al.*, 1979 ; *Takano and Liou*, 1989], and (2) more complex polycrystalline particles [*Macke et al.*, 1996] which were used for ISCCP ice cloud optical depth retrieval. It should be noted that we used the symbol Q instead of Q_{sr} in our figures.

The complete scattering matrix has been computed for randomly oriented particles having these shapes, by using a ray-tracing method supplemented by Fraunhofer diffraction (cf. *Macke et al.* [1996] for the polycrystals and *Brogniez* [1988] and *Chepfer* [1997] for the hexagonal particles). At the wavelength used (865 nm), the absorption by ice is very low [*Warren et al.*, 1986, 1988], hence the single-scattering albedo is close to 1. The scattering matrix is employed in a doubling-adding radiative transfer code [*De Haan et al.*, 1986] in order to take into account multiple scattering in the atmosphere. These radiative transfer computations yield the Stokes parameters of the emergent light at the top of the plane-parallel atmosphere, (I,Q,U,V). The normalized polarized radiance $L_{n,p}(\theta_v,\phi_v)$ is derived from these Stokes parameters as follows

$$L_{n,p}(\theta_v,\phi_s-\phi_v)=\frac{\pi\sqrt{Q^2+U^2+V^2}}{E_s}$$

where E_s is the incident solar flux at 865 nm at the top of the atmosphere, θ_v and ϕ_v are, respectively, the zenith and the azimuth viewing angles, and ϕ_s is the azimuth angle of the incident sunlight. According to the usual convention, $(\phi_s-\phi_v)$ is equal to 0° and 180° for forward and backward directions, respectively. The normalized total radiance (L_n) is derived from the first element (I) of the Stokes vector in the following manner

$$L_n(\theta_v,\phi_s-\phi_v)=\frac{\pi I}{E_s} \quad (2)$$

The quantities used in this study are the normalized polarized radiances ($L_{n,p}$) and the normalized total radiances (L_n), which are directly measured by POLDER. The normalized polarized radiance $L_{n,p}(\theta_v,\phi_s-\phi_v)$ and the normalized total radiance are, respectively, linked to the polarized reflectance $\rho_p(\theta_v,\phi_s-\phi_v)$ and the total reflectance $\rho_p(\theta_v,\phi_s-\phi_v)$ as follows:

$$\rho_p(\theta_v,\phi_s-\phi_v)=\frac{L_{n,p}(\theta_v,\phi_s-\phi_v)}{\mu_s} \quad (3)$$

$$\rho\,(\theta_v,\phi_s-\phi_v)=\frac{L_n(\theta_v,\phi_s-\phi_v)}{\mu_s} \quad (4)$$

where μ_s is the cosine of the solar zenith angle.

3.2. Simulations

In this sub-section, simulated values of normalized polarized radiances at 865 nm are presented for cirrus clouds. Results for various ice crystal shapes, different viewing geometries, and several solar zenith angles are given in order to describe the sensitivity of the polarized signal to these parameters. A wavelength of 865 nm is used because the contribution of scattering by molecules located above cirrus clouds is low at this wavelength. As an example, for a cirrus cloud top located at 530 hPa, the contribution of Rayleigh scattering to the normalized polarized radiance reaches a maximum of 0.0022 for a solar zenith angle equal to 40°. This contribution decreases with the cloud pressure. As we do not have reliable information on the cirrus cloud top pressure observed with POLDER, we have chosen to neglect the contribution of the Rayleigh scattering in our computations and consider it as an uncertainty.

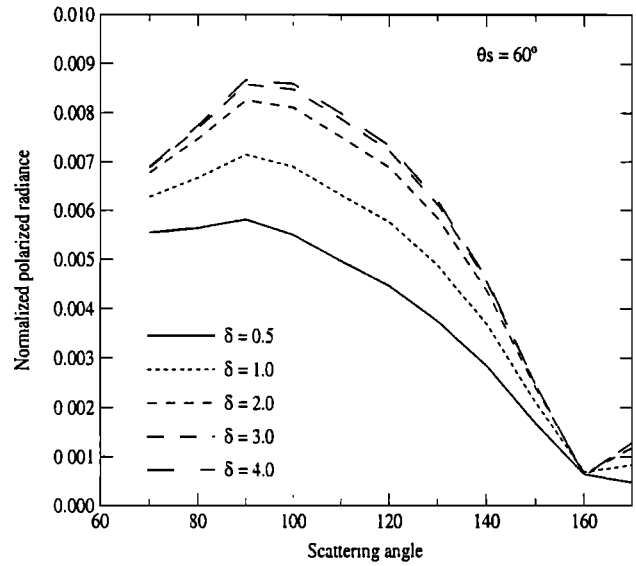

Figure 2. Simulated values of the normalized polarized radiance reflected by a cirrus cloud as a function of the cloud optical depth δ. The cloud is composed of polycrystalline particles.

Figure 2 depicts the normalized polarized radiance (compare equation (1)) as a function of the scattering angle for cirrus clouds composed of polycrystals. The albedo of single scattering is one, and the underlying surface is black. Results for different values of the cloud optical depth δ, between 0.5 and 4, have been plotted. Further, a constant solar zenith angle equal of 60° and a viewing direction in the solar principal plane ($\phi_s-\phi_v$ = 0°) have been assumed. Figure 2 shows that the normalized polarized radiance increases with the cloud optical depth until it saturates for optical depths higher than 4. For thicker clouds the polarized radiance is independent of the optical depth.

The normalized polarized radiance has been computed for different particle shapes in order to study the sensitivity of the signal to the particle type. The cloud optical depth was chosen to be 5 to ensure a saturated signal. Plate 1 shows polar diagrams of the saturated normalized polarized radiance ($L_{n,p}^{sat}$) computed for hexagonal compact crystals with a shape ratio Q_{sr}=1, hexagonal columns with Q_{sr}=2.5, polycrystalline particles, hexagonal plates with Q_{sr}=0.1, and hexagonal plates with Q_{sr}=0.05. This plate illustrates the high sensitivity of the saturated normalized polarized radiance to the ice crystal shape. The high sensitivity of the polarization to the particle shape was also revealed by lidar linear depolarization observations [*Sassen*, 1991]. That $L_{n,p}$ is much more sensitive to particle shape than the normalized total radiance (L_n) was also found with the airborne version of POLDER during EUCREX'94 [*Chepfer et al.*, 1998]. The space-

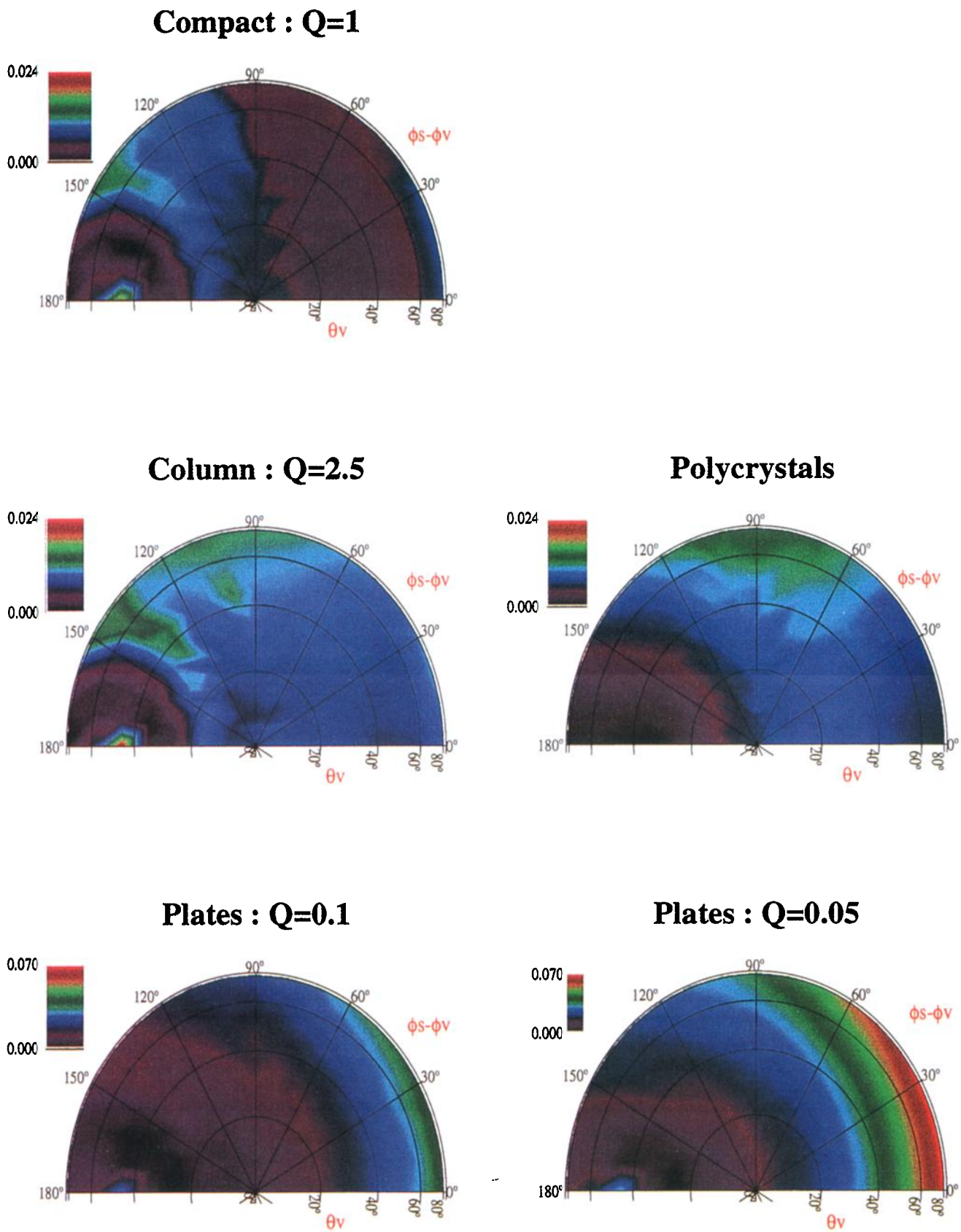

Plate 1. Calculated values of the saturated normalized polarized radiance for a cirrus cloud composed of various particle shapes: (a) hexagonal compacts (Q_{st}=1), (b) hexagonal columns (Q_{st}=2.5), (c) polycrystalline particles, (d) hexagonal plates (Q_{st}=0.1), and (e) hexagonal plates (Q_{st}=0.05). The solar zenith angle is 57.5°.

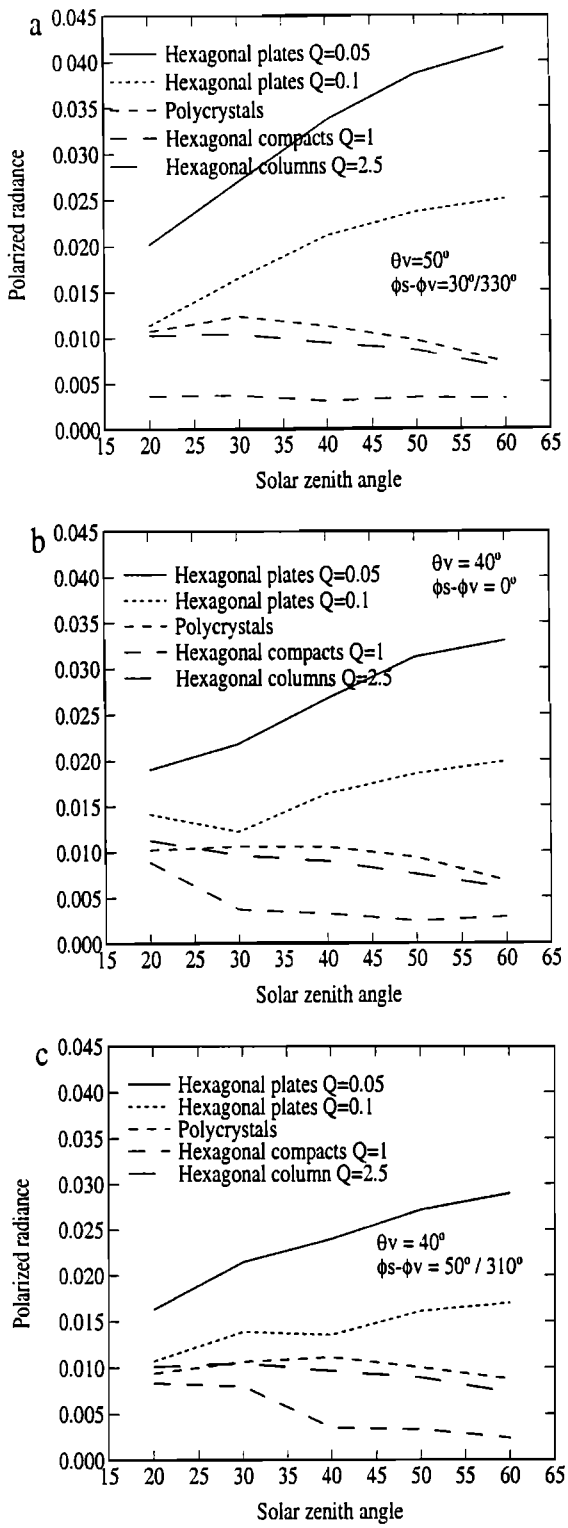

Figure 3. Saturated normalized polarized radiance as a function of the solar zenith angle for different ice crystal shapes and various viewing directions : (a) θ_v= 50°; ϕ_s-ϕ_v= 30° or 330°, (b) θ_v= 40° ; ϕ_s-ϕ_v= 0° , (c) θ_v= 40° ; ϕ_s-ϕ_v= 50° or 310° .

borne version of POLDER measures normalized radiance in viewing directions for which the viewing angles (θ_v) are smaller than 60°. For these viewing angles, Plate 1 shows that $L_{n,p}^{sat}$ is most sensitive to the particle shape for viewing directions comprised in the following angle boxes: 35°< θ_v <55° and 0°< ϕ_v <50° and in the corresponding directions that are symmetric with respect to the solar principal plane: 35°< θ_v <55° and 310°< ϕ_v <360°. Measurements of the normalized polarized radiances in these viewing directions are best suited to discriminate between the shapes of the ice crystals.

Figure 3 shows the variation of the saturated normalized polarized radiance with solar zenith angle for the particle shapes considered in this study. Figures 3a, 3b, and 3c pertain to the viewing directions (θ_v= 50; ϕ_s-ϕ_v= 30° or 330°), (θ_v= 40° ; ϕ_s-ϕ_v= 0°), and (θ_v= 40° ; ϕ_s-ϕ_v=50° or 310°), respectively. These three examples illustrate that the normalized polarized radiance can be used to discriminate between the different ice crystal shapes in cirrus clouds and that this discrimination is easier for high values of solar zenith angles (θ_s=60°) than for low ones (θ_s=20°). Figure 3 also shows that the distinction between polycrystalline particles and hexagonal columns (Q_{sr}=2.5) is difficult when we consider the uncertainty induced by ignoring Rayleigh scattering, which yields an error $\Delta L_{n,p}$=0.0022.

In the following sections the POLDER-saturated normalized polarized radiances measured above cirrus clouds are compared to calculated values to infer a global map of ice crystal shapes. In comparison to the normalized total radiance (L_n), the saturated normalized polarized radiance ($L_{n,p}^{sat}$) has the advantage of being independent of the cirrus cloud optical depth. As soon as the cloud optical depth is higher than 4, it only depends on the viewing geometry and the solar zenith angle. Consequently, the particle shape obtained by comparing saturated normalized polarized radiance observations and simulated values concerns only the upper layer of the cirrus clouds (i.e., the first few orders of scattering).

4. Selection of POLDER Observations

The detection of ice cloud pixels well suited for ice crystal shape determination is based on successive tests on the normalized total radiances and normalized polarized radiances collected by POLDER. The first test concerns the cloud detection (cloudy pixels), the second test concerns the cloud thermodynamical phase which in the present study is used to select ice clouds only, the third and fourth tests are applied to select cirrus clouds composed of ice crystals randomly oriented in space. These different tests are briefly described below (for more details, see *Chepfer et al.* [1999]).

1. The first test aims at selecting cloudy pixels located above oceans or sea surfaces and above land surfaces. Cloud detection above oceans consists in selecting pixels with bidirectional reflectances higher than a threshold value equal to 40%. This threshold value is safe enough to reject clear sky pixels and pixels corresponding to optically thin clouds. For pixels located above land surfaces, cloud detection is more complex because the ground reflectance varies strongly depending on the surface type (snow, desert, vegetation). We used a cloud detection scheme that has been specially developed for POLDER measurements over land surfaces by *Bréon et al.* [1999]. The use of this scheme for the current application is described by *Chepfer et al.* [1999].

2. The second test consists of identifying the cloud thermodynamical phase (ice or liquid water) in order to select ice cloud pixels and reject liquid water cloud pixels. This test was developed by *Goloub et al.* [1994] who used POLDER- polarized radiances measured at 865 nm. It is based on (1) the presence (or absence) of a peak at scattering angles around 140° and (2) the behaviour of the normalized polarized radiances for scattering

angles smaller than 110°. The results of this thermodynamical cloud phase test [*Goloub et al.*, 1994] have been compared with lidar measurements [*Chepfer et al.*, 2000] for validation. Further, *Goloub et al.* [2000] showed that this test selects ice clouds for which the normalized polarized radiance is saturated.

3.The third and fourth tests aim at selecting ice clouds composed of particles randomly oriented in space. The third test aims at selecting pixels for which the POLDER views the direction of specular reflection. POLDER observes a given target in 12 to 14 different directions. To detect specular reflection, these directions have to include (1) the specular reflection direction itself, which corresponds to a viewing zenith angle (θ_v) equal to a solar zenith angle (θ_s) in the solar principal plane (ϕ_s-ϕ_v=180°), and (2) neighboring directions to detect the presence of a peak. These geometrical constraints strongly reduce the number of pixels available for this study. The fourth test enables us to detect clouds composed of particles randomly oriented in space. It consists in removing pixels for which the polarized normalized radiance presents a peak in the specular direction. The peak is identified when the bi-directional normalized polarized radiance in the specular ($L_{n,p,\mathrm{spec}}$) direction (+/- 2°) has a greater value than the bidirectional normalized polarized radiance in the following ($L_{n,p,\mathrm{spec+1}}$) and previous ($L_{n,p,\mathrm{spec-1}}$) directions measured with POLDER. Hence if

$$(L_{n,p,\mathrm{spec}}-L_{n,p,\mathrm{spec-1}}) > 0 \quad (L_{n,p,\mathrm{spec}}-L_{n,p,\mathrm{spec+1}}) > 0, \quad (5)$$

a specular reflection peak is declared to be present. A previous study has been devoted to the quantity of particles preferentially orientated in space [*Chepfer et al.*, 1999]. In contrast, when the inequalities given in equation (5) are not satisfied, the cirrus cloud is considered to be composed of particles randomly oriented in space, and the pixel is selected for the particle shape determination.

The various tests described above enable selection of pixels corresponding to thick ice clouds for which the ice crystals can be assumed randomly oriented. For those pixels the saturated normalized polarized radiances measured with POLDER can be compared with simulated values (compare section 3) in order to characterize the shape of ice crystals.

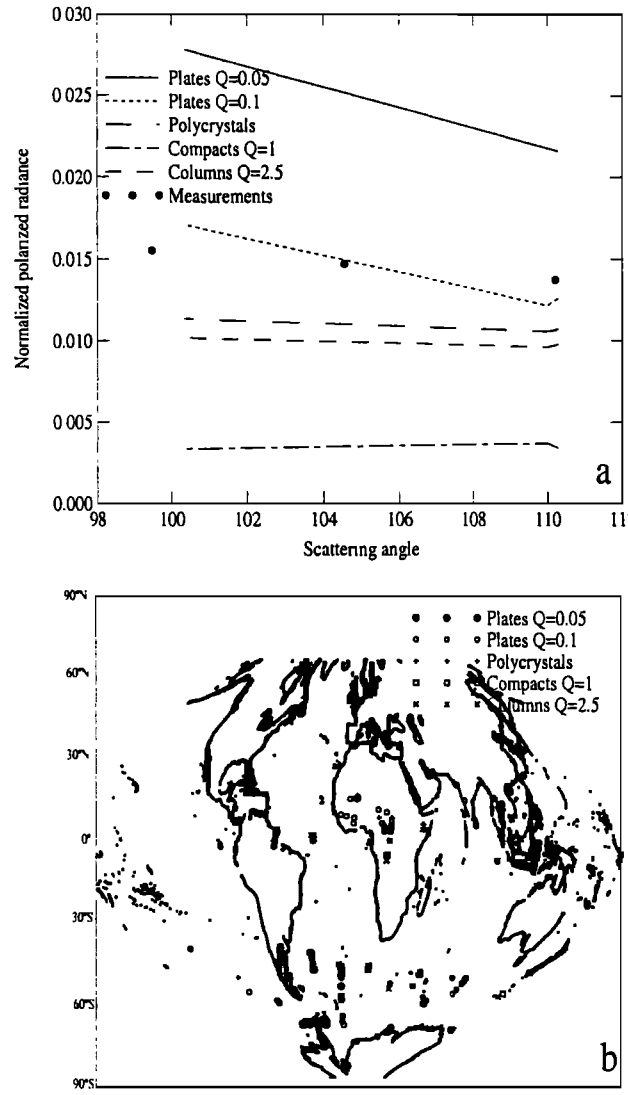

Figure 4. (a) Comparisons between saturated normalized polarized radiances simulated and observed with POLDER over a thick cirrus cloud. (b) Map of particle shapes randomly oriented in space for January 2, 1997.

5. Results

5.1. Test Case

Pixels pertaining to thick ice clouds whose ice crystals and randomly oriented in space have been selected employing the tests described above (section 4) for January 2, 1997. Only 4082 pixels [*Chepfer at al.*, 1999] can be used for crystal shape retrieval. The pixels are classified in boxes of viewing angles and solar zenith angles with 10° bin size in order to be compared with simulations corresponding to the same viewing and solar zenith angle conditions at +/- 5° (section 2b). Then differences between the saturated polarized radiance measured with POLDER and the corresponding simulated values are computed for each of the five ice crystal shapes. Finally, the pixel is flagged with the ice crystal shape for which the difference between the simulated and the observed values is minimal. In the case of a minimal difference larger than 0.01, the pixel is rejected.

When the POLDER instrument sees one pixel in 14 different viewing directions, the shape retrieval procedure is applied to each suitable direction. Next, for a given pixel, a quality indicator (α) is computed for each shape model. We use $\alpha=N_i/N_{tot}$, where N_i is the number of times for which the shape " i " has been obtained, and N_{tot} is the total number of shape retrievals for the pixel concerned. Finally, for a given pixel, the retrieved shape is considered reliable if $N_{tot} \geq 2$ and $\alpha > 0.5$. Usually, N_{tot} takes values between 2 and 5, and α is higher than two thirds. This test reduces the number of pixels for which the ice crystal shape is retrieved, but it prevents nonreliable shape retrievals.

Figure 4a shows an example of comparisons between observations and simulations for one pixel observed on January 2, where θ_s = 34°. The saturated normalized polarized radiance simulated for the appropriate viewing directions is plotted as a function of the scattering angle for the five different shapes. In this case the pixel is observed for three different directions (N_{tot} = 3) corresponding to the big dots in Figure 4a. Each of these observations is compared to simulations and flagged with the particle shape that agrees best. For example, Figure 4a shows that all three observations are flagged as " plates Q_{sr}=0.1. ". Further, this retrieval is considered reliable because the quality factor α=3/3=1.

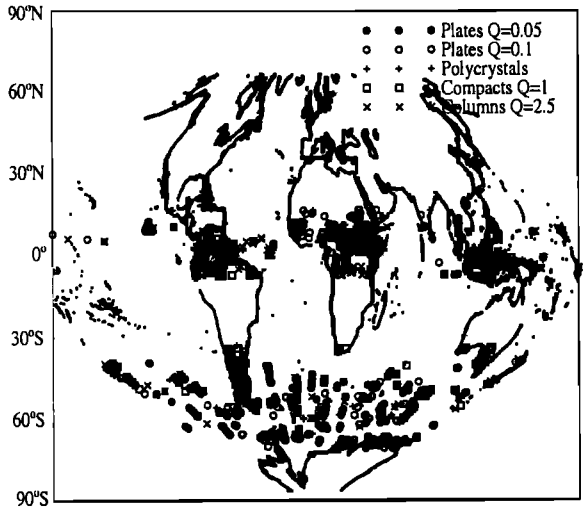

Figure 5. Map of particle shapes for a 6-day period in January 1997.

Repeating these comparisons for each selected pixel yields a map of ice crystal shapes for January 2, 1997 (Figure 4b). This map shows that few pixels can be used for the shape retrieval. As shown in Figure 4b, closely spaced pixels can correspond to different particle shape. The heterogeneous geographical distribution of these pixels is the result of the successive tests applied to the POLDER observations (section 4b), namely, (1) only latitudes between 90°S and 40°N were covered in January, (2) only ice clouds pixels were selected, (3) only pixels corresponding to cirrus clouds composed of particles randomly oriented in space have been used for this study (i.e., the specular direction needs to be observed, and the specular reflection peak has to be absent), (4) only pixels with viewing geometries sensitive to the particle shape (in polarization) have been retained.

5.2. Analyzing six Periods of 6 Days

To obtain more information about the global distribution of ice crystal shapes, we have processed six periods pertaining to 6 days collected in January, February, March, April, May, and June 1997.

Figure 5 presents the results obtained for the period January 1-6, 1997, and confirms the latitudinal distribution of the pixels used for the particle shape retrieval. This distribution is mainly due to the constraints on POLDER viewing geometry imposed by the selection procedure. In addition, it shows a lack of continuity between pixels located above land and above ocean surfaces, which is probably due to the different cloud detection schemes used above land and sea. A main difference between the schemes is that the cirrus clouds retained for the shape retrieval are very thick above oceans in order to avoid sea glitter and to properly determine the ice crystal orientation in space.

To obtain information about the latitude variation of the particle shape, 30° latitude intervals are considered and a histogram is made of the retrieved shapes in each interval. Figure 6a shows the number of pixels used for the shape retrieval for each latitude interval. Figures 6b to 6e show the percentage of each shape retrieved in each latitude interval. In January the Intertropical Convergence Zone (ITCZ) is located between 0° and 30° south, and the columns dominate there (Figure 6c). The two histograms corresponding to the adjacent latitude intervals (Figures 6b and 6d) are highly similar, showing that the dominant particle shape composing cirrus clouds is symmetrical with respect to the ITCZ. Figure 6e shows that at high latitudes the hexagonal plates occur more frequently compared to low latitudes.

The results obtained in the period June 1-6, 1997, are presented in Figure 7a to 7e. In that period the ITCZ was located in the 0°-30°N interval. The dominating ice crystal shape in that interval is the hexagonal compacts (Q_{sr}=1) and the column shape is the second most frequent. In contrast to January, in June the dominant ice crystal shape is not the same in the adjacent latitude bands (Figures 7c and 7d). Plates (Qsr=0.1) are dominant in the 30° to 60°N latitude band, whereas the columns are dominant in the 0° to 30° S band. As in January, the dominant particle shapes at high latitudes (Figure 7e) are the plates and polycrystals.

The results obtained for six different periods of 6 days are presented in Table 1. The polycrystals and hexagonal columns are classified in one single category since their polarization signatures are nearly the same (section 3.2). Table 1 shows that in general, the polycrystals and hexagonal columns occur most frequently globally, whereas at high latitudes the hexagonal plates occur more frequently. Table 2 summarizes mean occurrences of the different shapes for all periods considered and confirms the above results.

6. Discussion

Several points concerning the results mentioned above will be addressed here.

1. On the one hand, the accuracy of the polarized radiance measured with POLDER is better than 0.001, so measurement inaccuracies will not affect the shape retrieval significantly. On the other hand, the POLDER spatial resolution is 6x6 km at nadir, which means that the retrieved shape is an average shape corresponding to an area of at least 6x6 km.

2. The observations have been compared to several apriori models. In this respect, two remarks are in order. (1) The shape retrieval concerns only cirrus clouds composed of randomly oriented ice crystals, because the radiative transfer code that we used assumes random orientation in space of the scattering particles. Selecting pixels with randomly oriented ice crystals strongly reduces the number of pixels available for shape retrieval. In the future a similar method could be used to retrieve the shape of ice crystals that are horizontally oriented in space, as soon as radiative transfer codes become available that are able to handle such oriented particles. (2) Five different models for the ice crystal shapes have been considered. We do not pretend to reproduce all the cases encountered in nature. Nevertheless, we have noted that in most cases the polarized signature can be reproduced by one of the models considered. In the future, other shapes, based on cloud microphysical models, could be taken into account (as soon as the complete scattering matrix becomes available) in order to obtain more realistic particle shapes.

3. Several insitu observations have shown that cirrus clouds are often composed of ice crystals with a mixture of particle shapes. Such cirrus clouds have not been considered in this study, as it would have added an additional degree of freedom to the calculations. Including a particle shape distribution would increase the number of possible solutions. Hence the retrieved shape is an effective or average particle shape except, perhaps, for particle shapes corresponding to the extreme curves shown in

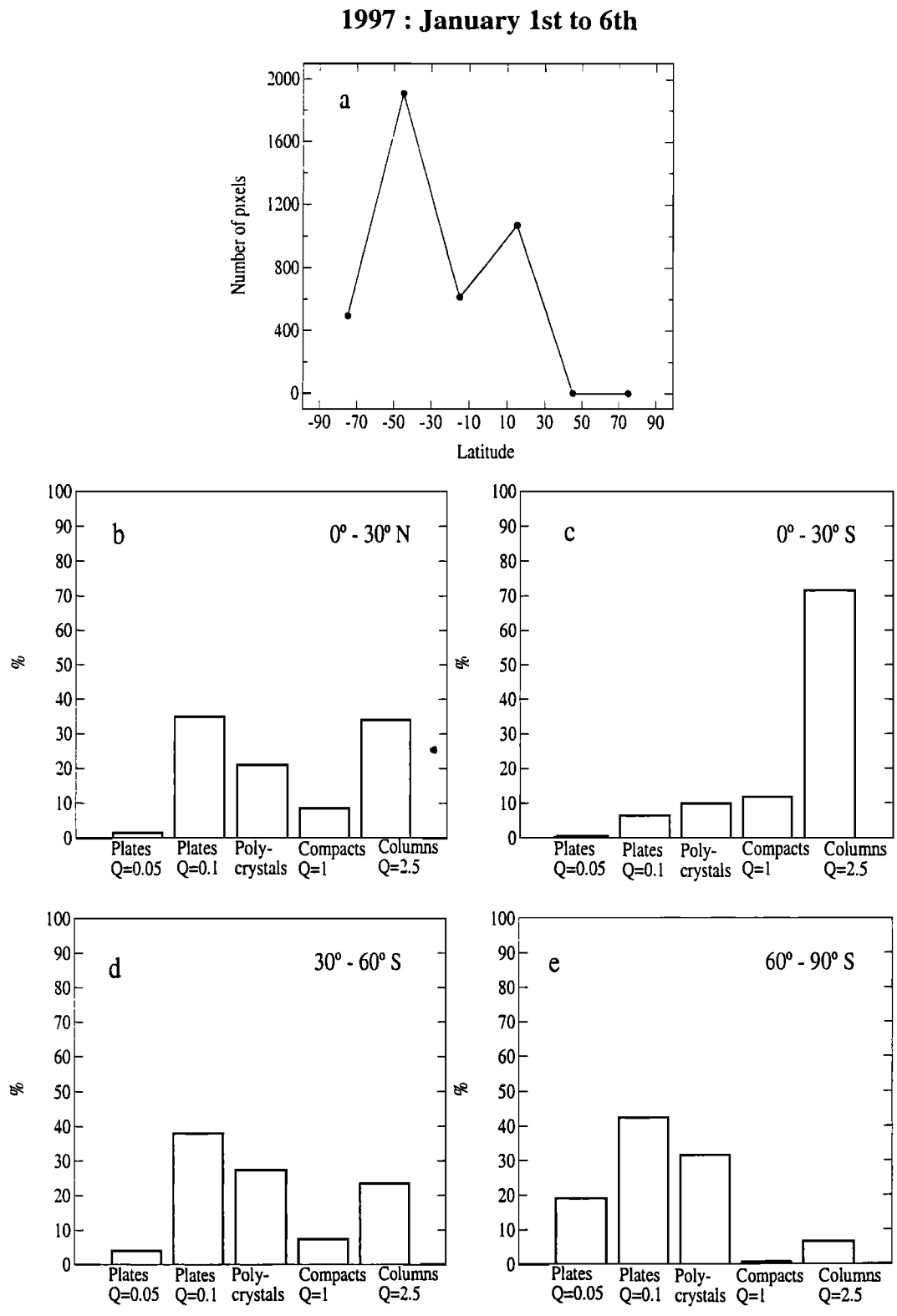

Figure 6. Latitudinal variation of the particle shape on a global scale in the period January 1-6 1997. (a) Number of pixels used for the shape retrieval as a function of latitude. (b-e) Histograms showing the relative occurrence (in percent) of the retrieved particle shape. Results for four latitude bands (width 30°) are given.

Figure 3, i.e., hexagonal plates (Q_{sr}=0.05) and hexagonal compact (Q_{sr}=1). For other retrieved particle shapes, the cirrus cloud might actually consist of a mixture of various particle types.

4. The particle shapes retrieved with POLDER have to be validated in the future. The field experiments discussed in section 1 have shown a wide variability of the particle shapes in cirrus clouds, including sometimes ideal shapes like hexagonal plates or columns and polycrystals. The particle shapes considered in this paper are plausible, as they correspond to particle types that have been observed in nature. Nevertheless, these results are currently difficult to validate rigorously, because no collocated in situ

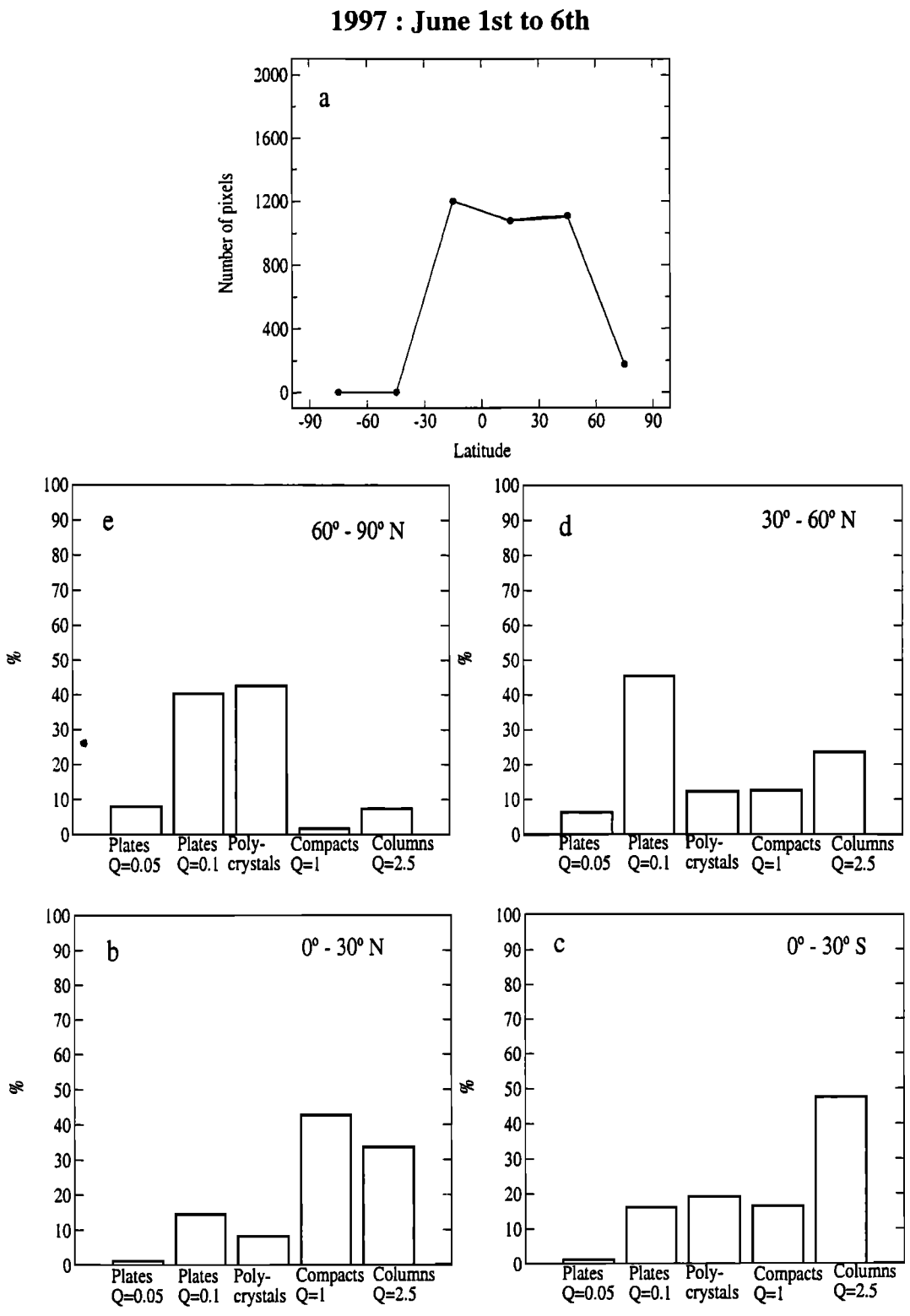

Figure 7. Same as Figure 6, but for the period June 1-6, 1997.

observations have been done in cirrus cloud during the POLDER-1/ADEOS-1 mission. Hence future validation is required using two approaches: (1) comparisons with in situ microphysical samples collected with an aircraft in cirrus clouds during the POLDER-2/ADEOS-2 mission, (2) comparisons with retrieved shapes deduced from forthcoming space-borne observations, using retrieval techniques based on other physical methods.

7. Conclusions

In this paper, normalized polarized radiance observations obtained with POLDER have been used to retrieve the shape of ice crystals that compose cirrus clouds. The method applied in this study is completely new as it uses polarization to retrieve the ice crystal shape. This method has three main advantages in

Table 1. Latitudinal Variation of the Frequency Distribution of Retrieved Particle Shapes

Period	Latitude	Number of Pixels	Plates Q_{sr}=0.05 (%)	Plates Q_{sr}=0.1 (%)	Columns (Q_{sr}=2.5) and Polycrystals (%)	Compacts Q_{sr}=1 (%)
January	90-60 N	0	0	0	0	0
1-6	60-30 N	0	0	0	0	0
	30-0 N	924	1	35	(55)	9
	0-30 S	509	0	6	(82)	12
	30-60 S	1423	4	38	(50)	7
	60-90 S	348	19	(42)	37	1
February	90-60 N	0	0	0	0	0
7-12	60-30 N	0	0	0	0	0
	30-0 N	1614	12	(61)	26	1
	0-30 S	173	4	23	(56)	17
	30-60 S	821	2	22	(72)	5
	60-90 S	12	0	(67)	33	0
March	90-60 N	0	0	0	0	0
19-24	60-30 N	629	1	24	(74)	1
	30-0 N	323	2	41	(53)	4
	0-30 S	882	2	24	(60)	13
	30-60 S	439	2	21	(74)	3
	60-90 S	0	0	0	0	0
April	90-60 N	0	0	0	0	0
18-23	60-30 N	1008	5	(47)	44	15
	30-0 N	0	0	0	0	0
	0-30 S	1307	3	18	(65)	15
	30-60 S	63	0	8	(89)	3
	60-90 S	0	0	0	0	0
May	90-60 N	0	0	0	0	0
	60-30 N	578	5	(46)	44	6
	30-0 N	214	1	24	(40)	36
	0-30 S	774	9	21	(57)	14
	30-60 S	0	0	0	0	0
	60-90 S	0	0	0	0	0
June	90-60 N	176	8	40	(50)	2
1-6	60-30 N	1108	6	(45)	36	13
	30-0 N	1078	1	14	42	(43)
	0-30 S	1201	1	16	(66)	16
	30-60 S	0	0	0	0	0
	60-90 S	0	0	0	0	0

In each latitude band, the dominant shape is listed in parentheses.

comparison with methods based on normalized total radiance (L_n) observations: (1) the normalized polarized radiance ($L_{n,p}$) is much more sensitive to a change in particle shape than the normalized total radiance, (2) the normalized polarized radiance ($L_{n,p}$) allows discrimination between ice and liquid clouds, without additional information on the cloud temperature or altitude, and (3) the normalized polarized radiance is saturated after a few scattering events and therefore independent of the cloud optical depth provided the cirrus cloud is sufficiently thick. Thus one degree of freedom has been removed from the shape retrieval procedure, as compared to a method based on total normalized radiance (L_n) observations. The main limitation of the method is that the retrieved particle shape pertains to ice crystals contained in the higher sublayers of the clouds.

This study is based on analyzing observations collected during six periods of 6 days in January, February, March, April, May, and June 1997. It is shown that the shape of ice crystals varies strongly spatially. Our analysis yielded the following conclusions: (1) the distribution of ice particle shape seems to be symmetric on both sides of the ITCZ (at least in January), (2) the polycrystals and hexagonal columns seem to dominante at low latitudes, whereas the hexagonal plates seems to occur more frequently at high latitudes. This latitudinal distribution of ice particle shapes may be due to the conditions during formation of

Table 2. Same As Table 1, But Averaged Over All Periods of 6 Days Considered (January, February, March, April, May and June 1997)

Latitude	Number of Pixels	Plates Q_{sr}=0.05 (%)	Plate Q_{sr}=0.1 (%)	Columns (Q_{sr}=2.5) and Polycrystals (%)	Compacts Q_{sr}=1 (%)
90°-60° N	176	8	40	(50)	2
60°-30° N	3323	4.5	42	(47)	7
30°-0° N	4156	5	(39.5)	(39.5)	16
0°-30° S	1710	3	18	(64.5)	14.5
30°-60° S	2746	3	30	(61)	6
60°-90° S	360	18	(43)	39	0

the cirrus clouds: at low latitudes, cirrus are often (but not always) the result of convection, whereas at middle and high latitudes, they are often associated with fronts but can also be generated by convection. The results obtained at low latitudes are consistent with the study of *Baran et al.* [1999] who used ATSR observations and concluded that near the top of tropical cirrus clouds, columns and polycrystals are most likely to occur.

In a follow-up study the 8 months of POLDER observations might be analyzed in order to obtain more data on the natural variability of the shape of ice crystals in cirrus cloud on a global scale. Finally, the next launch of ADEOS-2 and EOS-AM should provide the opportunity to derive global maps of crystal shape simultaneously with different instruments using independent retrieval methods, in order to validate the latitudinal shape distribution obtained in the present study.

Acknowledgments. We are indebted to A. Macke for providing us with the scattering matrix of polycrystals. The results presented here were obtained using a subset of the overall data set collected by the CNES's POLDER radiometer onboard the NASDA ADEOS.

References

Arnott, W. P., Y. Dong, and J. Hallet, The role of small ice crystals in radiative properties of cirrus: A case study, FIRE II, November 22, 1991, *J. Geophys. Res., 99*, 1371-1381, 1994.

Baran, A. J., S. J. Brown, J. S. Foot, and D. L. Mitchell, Retrieval of tropical cirrus thermal optical depth, crystal size and shape using a dual view instrument at 3.7 mm and 10.8 mm, *J. Atmos. Sci,* in press, 2000.

Bréon, F.-M., and S. Colzy, Cloud detection from the spaceborne POLDER instrument and validation against synoptic observations, *J. Appl. Meteorol., 38*, 777-785, 1999.

Brogniez, G., Light scattering by finite hexagonal crystals arbitrarily oriented in space, paper presented at the International Radiation Symposium, Lille, France. 18-24 August, 1988.

Brogniez, G., J. C. Buriez, V. Giraud, and C. Vanbauce, Determination of effective emittance and radiatively equivalent microphysical model of cirrus from ground-based and satellite observations during the International Cirrus Experiment : the 18 october 1989 case study, *Mon. Weather. Rev., 123*, 1025-1036, 1995.

Buriez, J. C., C. Vanbauce, F. Parol, P. Goloub, M. Herman, B. Bonnel, Y. Fouquart, P. Couvert, and G. Sèze, Cloud detection and derivation of cloud properties from POLDER , *Int. J. Remote. Sens., 18*, 2785-2813, 1997.

Chepfer, H., Etude théorique et expérimentale des propriétés optiques et radiatives des cirrus, Ph.D. thesis, 197 p., Lille Univ. 1997.

Chepfer, H., G. Brogniez, and Y. Fouquart, Cirrus clouds microphysical properties deduced from POLDER observations, *J. Quant. Spectrosc. Radiat. Transfer, 60*, 375-390, 1998.

Chepfer, H., G. Brogniez, P. Goloub, F-M. Bréon, P. H. Flamant, Cirrus cloud Ice crystals horizontally oriented in space observed with POLDER/ADEOS, *J. Quant. Spectrosc and Raiat. Transfer, 63*, 521-543, 1999.

Chepfer, H., P. Goloub, J. Spinhirne, P.H. Flamant, M. Lavorato, L. Sauvage, G. Brogniez, and J. Pelon, Cirrus clouds properties derived from POLDER-1/ADEOS polarized radiances: First validation using a ground-based lidar network, *J. Appl. Meteor., 39*, 154-168, 2000.

De Haan, J. F., P. B. Bosma, and J. W. Hovenier, The adding method for multiple scattering calculations of polarized light, *Astron. Astrophys.,183*, 371-391, 1986.

Deschamps, P. Y., F. M. Bréon, M. Leroy, A. Podaire, A. Brickaud, J. C. Buriez, and G. Sèze, The POLDER mission: Instrument characteristics and scientific objectives, *IEEE Trans. Geosci. Remote Sens., 32*, 598-615, 1994.

Deuzé, J. L., M . Herman, P. Goloub, D. Tanré, and A. Marchand, Characterization of aerosols over the ocean from POLDER/ADEOS-1, *Geophys. Res. Lett., 26(10)*, 1421-1424, 1999.

First ISCCP Regional Experiment (FIRE), *Mon. Weather Rev., 118*, 2259-2446, 1990.

Diner, D. J., G. P. Asner, R. Davies, Y. Knyazikhin, J. P. Muller, A. W. Nolin, B. Pinty, C. B. Schaaf, and J. Stroeve, New directions in Earth observing: Scientific applications of multiangle remote sensing, *Bull. Am. Meteorol., 80*, 2209-2228, 1999.

FIRE IFO II., *J. Atmos. Sci., 52*, 4041-4392, 1995.

Francis, P. N., A. Jones, R. W. Saunders, K. P. Shine, A. Slingo, and Z. Sun, An observational and theorical study of the radiative properties of cirrus: Some results from ICE'89, *Q. J. R. Meteorol. Soc.,120*, 809-848, 1994.

Giraud, V., J. C. Buriez, Y. Fouquart, and F. Parol, Large scale analysis of cirrus clouds from AVHRR data: Assesment of both a microphysical index and the cloud top temperature, *J. Appl. Meteorol.,36*, 664-675, 1997.

Goloub, P., J. L. Deuzé, M. Herman, and Y. Fouquart, Analysis of the POLDER polarization measurements performed over cloud covers, *IEEE Trans. Geosci. Rem. Sens., 32*, 78-88, 1994.

Goloub, P. M, Herman, H. Chepfer, J. Riedi, G. Brogniez, P. Couvert, and G. Sèze, Cloud thermodynamical phase classification from the POLDER spaceborne instrument, *J. Geophys. Res., 105(11)*, 14,747-14,759, 2000.

Hansen, J. E, Multiple scattering of polarized light in planetary atmospheres, part I, The doubling method, *J. Atmos. Sci., 28*, 120-125, 1971.

Herman, M., J.L. Deuzé, C. Devaux, P. Goloub, F.M. Bréon, and D. Tanré, Remote sensing of aerosols over land surfaces including polarization measurements: Application to some airborne POLDER measurements, *J. Geophys. Res., 102*, 17,039-17,049, 1997.

Heymsfield A. J., Cirrus uncinus generating cells and the evolution of cirriform clouds, part I, Aircraft observations of the growth of the ice phase, *J. Atmos. .Sci., 32*, 799-807, 1975.

Inoue, T., On the temperature and the effective emissivity determination of semitransparent cirrus clouds by bi-spectral measurements in the 10 μm window region, *J. Meteorol. Soc. Jpn., 63*, 88-98, 1985.

Krupp, C.,Holographic measurements of ice crystals in cirrus clouds during the International Cloud Experiment ICE 1989, in *Report of the 4th ICE/EUCREX Workshop,* Lab. d'Opt. Atmos., USTL, Lille, France, 1991.

Leroy, M., J.L. Deuzé, F.M. Bréon, O. Hautecoeur, M. Herman, J.C. Buriez, D. Tanré, S. Bouffiès, P. Chazette, and J.L. Roujean, Retrieval of atmospheric properties and surface bidirectional reflectances over the land from POLDER, *J. Geophys. Res., 102*, 17,023-17,037, 1997.

Liao, X., W. B. Rossow, and D. Rind, Comparison between SAGE II and ISCCP high-level clouds, 1, Global and zonal mean cloud amounts, *J. Geophys. Res., 100*, 1121-1135, 1995.

Liou, K. N., Review. Influence of cirrus clouds on weather and climate processes : A global perspective, *Mon. Weather Rev., 114*, 1167 – 1199, 1986.

Macke, A., J. Mueller, and E. Raschke, Single scattering properties of atmospheric ice crystal." *J. Atmos. Sci., 53*, 2813-1825, 1996.

McFarquhar, G. M., and A. J. Heymsfield, Microphysical characteristics of three cirrus anvils sampled during the Central Equatorial Pacific Experiment (CEPEX), *J. Atmos. Sci., 52*, 2401-2423, 1996.

Miloshevich, L. M., and A. J. Heymsfield, A balloon-borne cloud particle replicator for measuring vertical profiles of cloud microphysics: Instrument design and performance, in paper presented at the International Conference on Clouds and Precipitation, Zurich, 1996.

Minnis, P., K-N. Liou, and Y. Takano, Inference of cirrus cloud properties using satellite-observed visible and infrared radiances. part I, Parametrization of radiance fields, *J. Atmos. Sci., 50*, 1279-1304, 1993.

Minnis, P., Satellite remote sensing of cirrus: An overview, *paper presented at the International Conference on Cirrus*, Baltimore, Md., October 6-8, 1998.

Parol, F., J. C. Buriez, G. Brogniez, and Y. Fouquart, Information content of AVHRR channel 4 and 5 with respect to the effective radius of cirrus cloud particles, *J. Appl. Meteorol., 30*, 973-984, 1998.

Raschke, E., European Cloud and Radiation EXperiment (EUCREX), *final report,*, EV5V - CT 92 - 0130 EUCREX-2, 1996.

Raschke, E., P. Flamant, Y. Fouquart, P. Hignett, H. Isaka, P. R. Jonas, H. Sundquist, and P. Wendling, Cloud-radiation studies during the European Cloud Radiation Experiment (EUCREX), *Surv. Geophys., 19*, 89-138, 1998.

Rolland, P., and K. N. Liou, Remote sensing of optical and microphysical properties of cirrus clouds using MODIS channels, International Conference on Cirrus, Baltimore, Md., October 6-8, 1998.

Sassen, K., The polarization lidar technique for cloud research: A review and current assessment, *Bull. Am. Meteorol. Soc., 72*, 1848-1866, 1991.

Stephens, G. L., S. C. Tsay, P. W. Stackhouse Jr., and P. J. Flateau, The relevance of the microphysical and radiative properties of cirrus clouds to the climate and climatic feedback." *J. Atmos. Sci., 47*, 1742-1753, 1990.

SUCCESS, 2, Geophys. Res. Lett., *25*, 1327-1398, 1998.

Takano, Y., and K. N Liou, Solar radiative transfer in cirrus clouds. Part I : Single-scattering and optical properties of hexagonal ice crystals, *J. Atmos. Sci., 46*, 3-19, 1989.

Van de Hulst H. C., *Light Scattering by Small Particles*, 470 pp, Dover, Mineola, N.Y., 1957.

Vesperini, M., F.M. Bréon, and D. Tanré, Atmospheric water vapor content from spaceborne POLDER measurements, *IEEE* TGRS, 37, 1613-1619, 2000.

Warren, S. G., C. J. Hahn, J. London, R. M. Chervin, and R. Jenne, *NCAR Tech. Note, NCAR, TN-273 STR*, 212 pp., Natl. Cent. for Atmos. Res., Boulder, Colo., 1986.

Warren S. G., C. J. Hahn, J. London, R. M. Chervin, and R. Jenne, *NCAR Tech. Not, NCAR, TN-317 STR*, 212 pp., Natl. Cent. for Atmos. Res., Boulder, Colo., 1988.

Wendling, P., R. Wendling, and H. K. Weickmann, Scattering of solar radiation by hexagonal ice crystals, *Appl. Opt., 18*, 2663 – 2671, 1979.

H. Chepfer and P. Flamant, Laboratoire de Météorologie Dynamique, Ecole Polytechnique, 91128 Palaiseau Cedex, France. (chepfer@lmd.polytechnique.fr)

P. Goloub and J. Riedi, Laboratoire d'Optique Atmosphérique, Université de Lille I, 59655 Villeneuve d'Ascq Cedex, France.

J. De Haan and J. Hovenier, Department of Physics and Astronomy, Free University of Amsterdam, The Netherlands.

J. Hovenier, Astronomical Institute "Anton Pannekoek", University of Amsterdam, The Netherlands.

(Received September 29, 1999; revised March 16, 2000; accepted May 4, 2000.)